Published in final edited form as:
Clin Neurophysiol. 2018 May ; 129(5): 1001–1010. doi:10.1016/j.clinph.2018.01.075.

Intra-operative characterisation of subthalamic oscillations in Parkinson's disease

Xinyi Geng[a,b,g], **Xin Xu**[c], **Andreas Horn**[d], **Ningfei Li**[d,e], **Zhipei Ling**[c,*], **Peter Brown**[f], and **Shouyan Wang**[g,*]

[a]Suzhou Institute of Biomedical Engineering and Technology, Chinese Academy of Sciences, Suzhou, China

[b]University of Chinese Academy of Sciences, Beijing, China

[c]Department of Neurosurgery, Chinese PLA General Hospital, Beijing, China

[d]Department of Neurology, Movement Disorders Unit, Charité – University Medicine (CVK), Berlin, Germany

[e]Neural Information Processing Group, Institute of Software Engineering and Theoretical Computer Science, Technische Universität Berlin, Berlin, Germany

[f]MRC Brain Network Dynamics Unit, University of Oxford, Oxford, UK

[g]Institute of Science and Technology for Brain-Inspired Intelligence, Fudan University, Shanghai, China

Abstract

Objective—This study aims to use the activities recorded directly from the deep brain stimulation (DBS) electrode to address the focality and distinct nature of the local field potential (LFP) activities of different frequency.

Methods—Pre-operative and intra-operative magnetic resonance imaging (MRI) were acquired from patients with Parkinson's disease (PD) who underwent DBS in the subthalamic nucleus and intra-operative LFP recording at rest and during cued movements. Images were reconstructed and 3-D visualized using Lead-DBS® toolbox to determine the coordinates of contact. The resting spectral power and movement-related power modulation of LFP oscillations were estimated.

Results—Both subthalamic LFP activity recorded at rest and its modulation by movement had focal maxima in the alpha, beta and gamma bands. The spatial distribution of alpha band activity and its modulation was significantly different to that in the beta band. Moreover, there were significant differences in the scale and timing of movement related modulation across the frequency bands.

*Corresponding authors at: Department of Neurosurgery, General Hospital of PLA, 28 Fuxing Road, Haidian District, Beijing 100853, China (Z. Ling). Institute of Science and Technology for Brain-Inspired Intelligence, Fudan University, 220 Handan Road, Yangpu District, Shanghai 200433, China (S. Wang). lzp301hos@126.com (Z. Ling), shouyan@fudan.edu.cn (S. Wang).

Conflict of interest
Nothing to report.

Europe PMC Funders Author Manuscripts

Conclusion—Subthalamic LFP activities within specific frequency bands can be distinguished by spatial topography and pattern of movement related modulation.

Significance—Assessment of the frequency, focality and pattern of movement related modulation of subthalamic LFPs reveals a heterogeneity of neural population activity in this region. This could potentially be leveraged to finesse intra-operative targeting and post-operative contact selection.

Keywords

Intra-operative; Oscillation; Subthalamic nucleus (STN); Parkinson's disease (PD); Deep brain stimulation (DBS)

1 Introduction

There is growing interest in the nature of local field potential (LFP) activities recorded from the subthalamic nucleus (STN) of patients with Parkinson's disease (PD) undergoing neurosurgery for deep brain stimulation (DBS). This is fueled by the evidence that oscillatory activity in the beta frequency band is unduly synchronized and strong in these patients and that this relates to deficiency of dopamine in the basal ganglia (Hammond et al., 2007). Thus, the power of beta activity is correlated with the motor impairment in PD and the changes of power engendered by levodopa treatment or DBS correlate with improvements in bradykinesia and rigidity (Ray et al., 2008; Kühn et al., 2008, 2009; Eusebio et al., 2011). The same activities are modulated during the preparation, execution, and termination of voluntary movements (Kühn et al., 2004; Doyle et al., 2005; Klostermann et al., 2007; Joundi et al., 2012). However, the subthalamic LFP recorded in patients with Parkinson's disease also includes power in other frequency bands which are modulated by movement. Theta/alpha and gamma oscillations synchronise around the period of movement. Exaggerated theta/alpha activity has been related to the presence of dyskinesia and impulse control disorders (Alegre and Valencia, 2013; Rodriguez-Oroz et al., 2011). Similarly, gamma activity is associated with dyskinesias when it becomes exaggerated in the form of a finely tuned spectral peak (Fogelson et al., 2005; Swann et al., 2016).

The origin of these activities in the subthalamic area has been explored using intra-operative microelectrodes. This has led to the conclusion that beta activity is greatest in the dorsal 'motor' STN (Lourens et al., 2013; Verhagen et al., 2015). Importantly, these activities may also be evident in the LFP recorded directly from the definitive DBS electrode rather than from temporary microelectrodes. This has led to interest in exploiting LFP features to help improve functional targeting during surgery (Miyagi et al., 2009; Chen et al., 2006; Michmizos et al., 2015; Kolb et al., 2017; Yoshida et al., 2010), streamline the post-operative screening of electrode contacts (Tinkhauser et al., 2017) and form the basis of control signals in closed-loop DBS (Little et al., 2013). However, much still remains uncertain. To what extent are these subthalamic activities in different frequency bands focal when picked up by DBS electrodes rather than by microelectrodes? Are their sources separable in space? To what extent are spectral differences also associated with different patterns of modulation upon voluntary movement? Here we try to address these outstanding questions through an exploration of the spatial topography and movement-related reactivity

Europe PMC Funders Author Manuscripts

Europe PMC Funders Author Manuscripts

of spectral features recorded directly from bilateral subthalamic DBS electrodes in eight patients with Parkinson's disease.

2 Material and methods

2.1 Subjects and surgery

Eight patients (six males, age 54.6 ± 7.1 years) with Parkinson's disease underwent bilateral STN implantation of DBS electrodes at the General Hospital of PLA, Beijing, China. All patients gave written informed consent to take part in this study, which was agreed by the local ethics committees. The pre-operative Unified Parkinson's Disease Rating Scale part III – motor exam was evaluated one week before surgery (Table 1). Surgeries were performed after overnight withdrawal of levodopa in all patients.

All patients underwent stereotactic-framed pre-operative 3.0 T magnetic resonance imaging (MRI) scans the day before the surgery. The DBS electrodes were targeted at the dorsolateral area of the STN. The targets and trajectory of electrode implantation were calculated and determined using the Frame link planning station (Medtronic, Minneapolis, MN, USA). The DBS electrodes were Medtronic 3389 (Medtronic, Minneapolis, MN, USA) with four platinum-iridium cylindrical surface contacts. Each contact was 1.27 mm in diameter and 1.5 mm in length, and separated by 0.5 mm. The most caudal contact was contact 0 and the most rostral was contact 3. Subjects had local anesthesia and were awake during the operation to allow for intraoperative movement and stimulation assessments. The placement of DBS electrodes was confirmed intra-operatively by 1.5 T MRI (Cui et al., 2016) and macrostimulation effects.

2.2 Paradigm and recording

Bipolar LFPs were intraoperatively recorded from the adjacent four contacts (contact pairs: 01, 12, 23) of each DBS electrode. The recordings were made after the implantation of DBS electrodes on each side. All LFPs were band-pass filtered in the range of 0.1–500 Hz, amplified with a gain of 10,000, and sampled at 1000 Hz (EEG100C, BIOPAC Inc., USA). The signals were displayed online, saved onto a hard disk (Acqknowlege 4.2, BIOPAC Inc., USA), and exported for further analysis in MATLAB (MathWorks Inc., Natick, MA, USA).

Patients underwent recording at rest and during auditory-cued movement. Patients were instructed to avoid speaking during the tasks. During the movement task, patients were asked to hold a joystick handle with a button on top in the hand contralateral to the LFP recording. An auditory cue was delivered at random intervals ranging from 5 to 6 s. The patients were asked to click on the button using the thumb as fast as possible following the cue. The cueing sound was 100 ms spindle shaped white noise with 10% voltage ramp at the beginning and at the end. It was delivered through a speakerphone, adjusted so as patients volunteered that they could hear the cue clearly but did not feel it uncomfortable. The cue onset time was defined as the time of 50% of the ramp up. The response time was defined as the time of button press. The cue and button click were recorded by analog channels on the amplifier (UIM100C, BIOPAC Inc., USA). At least forty trials were performed for off-line analysis.

2.3 Signal processing

Data analyses were performed offline with custom developed scripts in MATLAB (MathWorks Inc., Natick, MA, USA). LFP signals were band-pass filtered over 3–90 Hz and adaptively band-stop filtered to reject 50 Hz line noise. The adaptive filter applied here used the power ratio of the stop-band and of reference sidebands to adjust the attenuation of the stop-band to avoid over-filtering. A continuous 60 s at rest and 30 trials of movement, free-of-artefact signals in all three bipolar contacts, were selected from each electrode after pre-processing.

Power spectral density (PSD) was calculated using the Welch's method (MATLAB function pwelch. Shimamoto et al., 2013; Welch, 1967) with 1 s sliding-window, 0.5 s overlap and 2048 points. The resting PSD was normalised across all contact-pairs of a given electrode at each frequency. The normalised power of contact-pair C_i on frequency f_j was calculated as $P_{normalise}(C_i, f_j) = \frac{P(C_i, f_j)}{1/3\sum_{i-1}^{3} P(C_i, f_j)}$.

Movement-related modulation of oscillations over 0–90 Hz were plotted as time-frequency spectrograms aligned to the time of cue, response onset and end of the movement. The time-frequency spectrograms were calculated using the short-time Fourier transform (STFT) with a 0.6 s sliding window and 0.005 s step. The length of the sliding window and its overlap were shorter than used for analysis of the resting signal. The impact of this however will have been lessened by the fact that power and reactivity estimates for both rest and movement data were normalised. Activities were extracted from each trial over the period 2 s prior to and 3 s after the clicking response. The time-frequency spectrograms of movement modulated oscillations were normalised to the baseline power taken as −1.2 to −0.2 s before the cue of each trial.

A cluster-based permutation test was performed to evaluate the statistical significance of movement-related changes in time-frequency spectrograms compared to baseline power at the group level. The pre-cluster threshold *P*-value was 0.01 and the permutation number was 1000. The actual *P*-values derived from permutation were corrected for multiple comparisons using the cluster-based approach with the pre-cluster threshold *P*-value.

The spectra were then averaged over the frequencies with significant movement- related power changes that occurred 0.2 s around the response time. To compare power changes between the low beta and high beta frequency bands, and between the low gamma and high gamma frequency bands, paired *t*-tests were performed at the group level. Significant differences in amplitudes of movement modulations are marked by yellow bars ($p < 0.01$, paired *t*-test).

2.4 Visualization of contact distribution

The preoperative and intra-operative MRI-scans were separately reconstructed and 3-D visualised by two researchers. The mean differences between the two observers in the x, y, and z coordinates were 0.52 ± 0.30 mm, 0.61 ± 0.44 mm and 0.51 ± 0.36 mm, respectively. The calculation and 3-D visualization were performed by the Lead-DBS toolbox (Horn and

Kühn, 2015; http://www.lead_dbs.org). The T1/T2-weighted pre-operative and T2-weighted intra-operative MRI-scans were fused and reconstructed to determine the position of DBS electrodes in relation to the subthalamic area. The MRI-scans were spatially normalised into the standardized MNI stereotactic space using the Statistical Parametrical Mapping (SPM) software version 12. The normalised images were then reconstructed with electrodes onto the MNI-space version of the Morel atlas (Jakab et al., 2012; Morel, 2013). The location of each electrode's contact was registered into x, y, and z coordinates in MNI-space, with these coordinates being averaged across the two observers. The bipolar recording location of LFP was then defined as the middle point of the pair of adjacent contacts and the coordinate was calculated accordingly.

2.5 Statistical analysis of power distribution

To evaluate whether sites sharing similar spectral power in different frequency bands formed clusters or not, we calculated the Euclidean distance between every two contact-pairs and compared the variances in Euclidean distance between the master group containing all contact-pairs ($N = 48$) and a subgroup ($n = 16$) of a third of contact-pairs selected on the basis that they had the highest ranked resting spectral power or movement related modulation. The hypothesis behind this was that those sixteen contact-pairs ranked highest would likely be sampling from a relatively circumscribed focus, whereas the remaining contact-pairs would be more distributed. The subgroup was regarded as clustered if a variance test of Euclidean distance between the subgroup and the master group was significant and the mean and standard deviation (SD) of Euclidean distances of the subgroup were smaller. The variance test used was the two-sample F-test for equal variances in MATLAB (function vartest2). This returns a test decision for the null hypothesis that the data in two vectors comes from a normal distribution with the same variance, using the two-sample F-test. The test rejects the null hypothesis at the significance level alpha, which in this case was 0.05 or less, as dictated by the false discovery rate procedure.

To compare whether the power distribution differed between frequency bands, the multivariate Kullback–Leibler divergences (KLD) were calculated (Kullback and Leibler, 1951; Sburlea et al., 2015). The KLD from a statistical discrete probability distribution Q to another distribution P is calculated as $KLD(P|Q) = \sum_i P(i) log \frac{P(i)}{Q(i)}$ where i = 1, 2, …, 48, representing the number of samples. The discrete probability distribution of an oscillation was calculated by taking the ratio of the spectral power of each contact-pair and the total power across all contact-pairs. In this way, the summation of the probabilities of the distribution would be 1 and the spectral power was registered as a probability in the distribution. The observed KLD between two distributions was compared with the KLDs of two permuted distributions with 1000 samples non-repetitively and randomly selected from the combined distribution. When the probability of the permuted KLDs being larger than that of the observed KLD was less than 0.05 (Prob {permuted KLD > observed KLD} < 0.05), the two distributions were considered as significantly different. Because the measurement of KLD is asymmetrical, the result of $KLD(P|Q)$ is different from $KLD(Q|P)$. The two power distributions were considered as significantly different only if the KLD measured in both directions were significant.

3 Results

3.1 Targeting

The location of contacts is shown in the 3-D visualized subthalamic area in Fig. 1. The coordinates of the forty-eight pairs of contacts in the eight subjects were estimated by taking the middle point of each contact-pair. These sites were then related to the location of the STN in MNI stereotactic space. 19/48 pairs of contacts were located inside STN, 13/48 pairs included the border of the STN and 16/48 pairs were outside of STN.

3.2 LFPs at rest

Peaks in low beta band power were found in at least one contact-pair in 12 sides, and had a mean frequency of 17 ± 2 Hz. Peaks in the high beta band were found in at least one contact-pair of all sides, and had a mean frequency of 28 ± 3 Hz (see example in Fig. 2B). Accordingly, the z-score normalised group averaged power spectral density of all sides showed a prominent peak in the low and high beta frequency band (Fig. 3A).

3.3 Is spectral power at rest localized within the subthalamic area?

An example of the distribution of oscillations in the subthalamic area at rest is shown in Fig. 2B. The contact-pair located in the dorsal STN showed the highest resting power in beta. The gradient in beta power across bipolar contacts in all sides and subjects was calculated to confirm that the beta activity was locally generated in the subthalamic area. The mean gradient in beta power from the contact-pair with maximum power to the remaining contact-pairs was 49.9% ± 8.9%. To further address whether spectral power at rest was localized within the subthalamic area we contrasted the location of the 16 bipolar contacts with the highest normalized power in a given band with that of all 48 contacts, based on the premise that sites selected for their high power might have a different distribution to unselected sites. The distribution of these 16 sites for the theta (4–8 Hz), alpha (8–12 Hz), low beta (13–20 Hz), high beta (21–32 Hz) and high gamma (60–90 Hz) bands is shown by the red dots in Fig. 3B–F. White dots are the remaining sites, with dots corresponding to the middle point between the contacts in a contact-pair. The numbers of sides and subjects involved in the subgroup of 16 are shown in Table 2. At least one contact-pair from each subject was included in the subgroup except in the case of high beta oscillations. The mean and standard deviation of the master group is 4.0 ± 1.9 mm (mean ± SD) and those of the selected subgroups are shown in Table 2. The mean and standard deviation of the Euclidean distances and the F-statistics and *P*-values of the variance test between the high power subgroup (n = 16) and the master group (n = 48) are shown in Table 2, and for those selected from each electrode are shown in Supplementary Table 1. High power sites were in a significantly tighter cluster than unselected sites in all frequency bands except for the theta and alpha bands. Clustering in the theta band was no different to that of unselected sites, but clustering in the alpha band was significantly less than for unselected sites. Similar findings were seen in the alpha (less focal) and high beta band (more focal) if we took contact-pairs with the highest relative power in each band from each electrode, rather than from across the group (see Supplementary Fig. 1 and Supplementary Table 1).

3.4 Are high power sites differentially located in different frequency bands?

Across all subjects, resting power distributions significantly differed in the theta and low beta bands, and in the alpha and high beta bands (Supplementary Table 2). In general, low beta power was more clustered in the STN than theta power, and gamma power extended more dorsally outside the STN than high beta power (Fig. 3).

3.5 Movement-related modulation of subthalamic oscillations

The time-frequency spectrograms of all recording channels in a −2 to +3 s window aligned to the response onset (t = 0) were normalised, group averaged and evaluated with a cluster-based permutation test to identify significant differences from baseline (Fig. 4A). Significant differences were found over the low (3–12 Hz), beta (16–36 Hz) and gamma (59–73 Hz) frequency bands within 0.2 s around response onset (Fig. 4A). The post-movement power increase was also greater than baseline over 12–29 Hz and 45–57 Hz.

Significant movement-related modulation in the whole beta frequency (13–32 Hz) band was found in 34/48 contact-pairs, with at least a 20% power decrease from the baseline (within subject paired *t*-test, $p < 0.01$). Significant power increases of at least 20% from the baseline were found in 18/48 contact-pairs over the gamma frequency (40–90 Hz) band (within subject paired *t*-test, $p < 0.01$). Within this range, power increases were found in 13/48 contact-pairs in the low gamma frequency (40–60 Hz) band and 11/48 contact-pairs in the high gamma frequency (60–90 Hz) band.

The range in movement-related power modulation differed between the low and high beta bands (Fig. 5B). Averaging across all recording channels, power changes during movement were found to be significantly different in the trough around the response and in the post-movement peak (Fig. 5B, yellow bars). Movement related power changes were greater for the high beta band (paired *t*-test, $p < 0.01$). However, the timing of the movement related power decrease and the duration of the trough-to-peak in these two bands was not significantly different (paired *t*-tests, $p > 0.01$). The power changes over the low and high gamma frequency bands were not different at response onset, but low gamma oscillations showed a more sustained increase after the end of the movement (Fig. 5C, paired *t*-test, $p < 0.01$).

3.6 Distribution of movement-related modulation in the subthalamic area

To better evaluate the movement-related modulations, oscillations in frequency bands with statistically significant power changes were analysed. The spectral power was calculated over the 0.2 s around the response within the cluster-permutation test defined significant voxels (Fig. 4). We contrasted the location of the 16 bipolar contacts with the highest power modulation in a given band with that of all 48 contacts (Fig. 4). The mean and standard deviation of the Euclidean distances and the F-statistics and *P*-values of the variance test between the highest power modulation subgroup ($n = 16$) and the master group ($n = 48$) are shown in Table 2. Sites with the greatest movement-related power modulation were in a significantly tighter cluster than unselected sites in all frequency bands except for the theta and gamma bands. Clustering in the theta band was no different to that of unselected sites, but clustering in the gamma band was significantly less than for unselected sites. Similar

findings were seen in the alpha (more focal) and low beta bands (more focal) if we took contact-pairs with the highest relative power in each band from each electrode, rather than from across the group (see Supplementary Table 1).

Significant differences were found between movement related modulation in the alpha band and that in the low beta and high beta bands (Supplementary Table 2). In general, alpha band power modulation was concentrated more ventrally in the STN than beta band power modulation (Fig. 4). The question also arises whether the distribution of maximal power and movement related reactivity in each band coincided across sides. To address this we performed a signed rank test on the contact-pair which ranked highest at rest and that with the greatest movement related modulation across the sides. *P*-values were $P\{\text{theta}\} = 0.0008$; $P\{\text{alpha}\} = 0.0011$; $P\{\text{low-beta}\} = 0.066$; $P\{\text{high-beta}\} = 0.0223$; and $P\{\text{gamma}\} = 0.001$. This suggests that the distributions of peak power and movement reactivity differed in the theta, alpha and gamma bands. Contrasting Figs. 3 and 4 suggests that alpha reactivity was more focussed in the ventral STN than alpha power at rest, and hence the mean Euclidean distance dropped during movement (Table 2). In contrast, gamma power at rest was maximal in dorsal STN and bordering zona incerta and gamma reactivity was more evenly distributed across the subthalamic area. Hence the mean Euclidean distance increased during movement (Table 2).

4 Discussion

We demonstrate that both subthalamic LFP activity recorded at rest and its modulation by movement have focal maxima in the beta band. The coordinates of these maxima correspond to the subthalamic nucleus. The picture was slightly more complicated in the alpha and gamma bands though. In the alpha band the peak power at rest was widely distributed and extended to include the zona incerta bordering the dorsal STN. However, upon movement reactivity in this band became more focal. The converse was seen in the gamma band, which was focal at rest, but became less clustered during movement, when reactivity extended to include the zona incerta.

The most parsimonious conclusion is that spectral activities and their modulation were locally generated, most likely at the level of the afferent input to the subthalamic region (Logothetis, 2003; Buzsaki et al., 2012). Critically, however, these focal activities were not uniform, but their precise character varied according to broad spectral divisions, and, in the case of the alpha and gamma band activities, whether rest or movement were considered. Indeed, the spatial distribution of alpha band activity and its modulation was significantly different to that in the beta band. Moreover, there were significant differences in the scale and timing of movement related modulation across the frequency bands. Within the beta band the depth of movement-related modulation was greater in the upper than lower frequency range. Within the gamma band modulation in the lower frequency range was more sustained than in the upper frequency band, lasting beyond the termination of movement. Considered together, these observations suggest that the spectral pattern of subthalamic LFP activity may contain information about the finer spatial and functional character of underlying neural population activity. This heterogeneity in local population activity was relatively consistent across patients in so far as it was evident in group level analyses, and

there was no significant difference between the distribution of resting power and movement-related modulation within the beta band.

4.1 Study limitations

Important limitations in the present study were that recordings were restricted to patients with PD, and so any inference with regard to normal physiological function must be considered speculative. Another limitation is that the phenotypic variability of the recruited patients could have influenced the distribution of the oscillations since some may be related to specific symptoms (Eusebio and Brown, 2007; Brittain and Brown, 2014). Furthermore, as our recordings were made intra-operatively and so may have been affected by stun or micro-lesion effects (Mestre et al., 2016). Nevertheless, we found peaks in beta activity in at least one channel on all sides. An additional issue is the relatively coarse spatial resolution of bipolar recordings made from the DBS macroelectrode, although despite this we were still able to record some differences in spatial topography between frequency bands. Finally, our findings are descriptive and unsupported by clinical correlations or evidence of direct mechanistic roles for different subthalamic oscillations. That said, the translational potential of the observations made here relate to the robustness of spatial and functional associations, which may still be essentially epiphenomenal.

4.2 Focality

Both focality and functional distinctions were seen despite the fact that LFP activity was captured through the bipolar contacts of DBS macroelectrodes and classified into somewhat arbitrary frequency bands. Bipolar recordings from adjacent electrode contacts are necessary to limit volume conduction from distant sources like cerebral cortex (Marmor et al., 2017), but, on the other hand, it must be conceded that the focality and functional distinctions disclosed in this study may hide an even finer level of organization in frequency and space. Data from microelectrode recordings support this view (Reck et al., 2009; Bour et al., 2015).

The focality of LFP signals recorded with DBS electrodes is beginning to be leveraged clinically, to assist intra-operative targeting (Chen et al., 2006; Miyagi et al., 2009) and support post-operative contact screening (Tinkhauser et al., 2017). Both approaches have focused on beta band activity, but the present findings suggest that spatial information may also be present in movement-induced modulation and resting power in the alpha and gamma bands, respectively. It remains to be seen whether there are additional advantages in considering all three bands, - alpha, beta and gamma, when it comes to predicting the best site for therapeutic stimulation. Our results suggest that the predictive value of alpha and gamma activity might depend upon whether peak power at rest or peak reactivity with movement are determined.

4.3 Heterogeneity in local population activity

The heterogeneity of subthalamic LFP activities is becoming increasingly apparent. Several functional and pharmacological differences have previously been reported between the low beta and high beta frequency bands (Levy et al., 2002; Doyle et al., 2005; Foffani et al., 2005; Joundi et al., 2012; Tan et al., 2013), although we found these sub-bands to share similar focality and reactivity. In the gamma band, finely-tuned gamma oscillations

Europe PMC Funders Author Manuscripts

associated with dyskinesias have been distinguished from broad gamma band activity and reactivity (Jenkinson et al., 2013). The latter is associated with elevated levels of arousal and movement vigor (Joundi et al., 2012; Anzak et al., 2012; Tan et al., 2013). Activity at the lower end of the gamma band has also been associated with parkinsonian tremor (Weinberger et al., 2009; Beudel et al., 2015), and here we show that this activity demonstrates a more sustained increase after movement than LFP activities at higher gamma frequencies.

The heterogeneity of subthalamic LFP activities is broadly consistent with the view that "tuning to distinct frequencies may provide a means of marking and segregating related processing, over and above any anatomical segregation of processing streams" (Fogelson et al., 2006). Thus, the spatial and functional distinctions between different spectral elements of the LFP identified here are complemented by evidence of frequency dependent differences in the coupling of subthalmic activities with other sites (Lalo et al., 2007; Fogelson et al., 2006; Litvak et al., 2011; Hirschmann et al., 2011). The potential clinical relevance of this is that both the local topography and frequency of subthalamic LFP activities might help identify different processing streams and this could be relevant in directing DBS to control different phenotypic features and avoid different stimulation-related side-effects (Horn et al., 2017). Supporting this view is the evidence that bradykinesia-rigidity, tremor and dyskinesias correlate with LFP activities of different frequency (Kühn et al., 2009; Weinberger et al., 2009; Rodriguez-Oroz et al., 2011; Beudel et al., 2015). Importantly, recent developments in DBS provide the means to realise the discriminative potential of spectral information through directed fields of stimulation (Pollo et al., 2014; Timmermann et al., 2015; Bour et al., 2015), specific temporal patterning of stimulation (Cagnan et al., 2017; Adamchic et al., 2014) and chronic recording of LFP activity to allow for pathophysiological changes over time (Steiner et al., 2017).

5 Conclusion

The results are consistent with heterogeneous population activities in the subthalamic region, as evidenced by differences in the focality and patterns of movement related modulation of specific spectral features of the LFP recorded intra-operatively in PD patients. The LFPs recorded with DBS electrodes in the STN are a rich source of information that could prove useful in better refining surgical targeting, contact selection and closed-loop therapy.

Supplementary Material

Refer to Web version on PubMed Central for supplementary material.

Funding sources

This work was supported by the National Natural Science Foundation of China [Grant No. 81471745]; the China Scholarship Council [Grant No. 201504910526]; Peter Brown was supported by the Medical Research Council (award MC_UU_12024/1).

References

Adamchic I, Hauptmann C, Barnikol UB, Pawelczyk N, Popovych O, Barnikol TT, et al. Coordinated reset neuromodulation for Parkinson's disease: proof-of-concept study. Mov Disord. 2014; 29(13): 1679–84. [PubMed: 24976001]

Alegre M, Valencia M. Oscillatory activity in the human basal ganglia: more than just beta, more than just Parkinson's disease. Exp Neurol. 2013; 248:183–6. [PubMed: 23764499]

Anzak A, Tan H, Pogosyan A, Foltynie T, Limousin P, Zrinzo L, et al. Subthalamic nucleus activity optimizes maximal effort motor responses in Parkinson's disease. Brain. 2012; 135:2766–78. [PubMed: 22858550]

Beudel M, Little S, Pogosyan A, Ashkan K, Foltynie T, Limousin P, et al. Tremor reduction by deep brain stimulation is associated with gamma power suppression in Parkinson's disease. Neuromodulation. 2015; 18:349–54. [PubMed: 25879998]

Buzsaki G, Anastassiou CA, Koch C. The origin of extracellular fields and currents–EEG, ECoG, LFP and spikes. Nat Rev Neurosci. 2012; 13:407–20. [PubMed: 22595786]

Bour LJ, Lourens MA, Verhagen R, de Bie RM, van den Munckhof P, Schuurman PR, et al. Directional recording of subthalamic spectral power densities in Parkinson's disease and the effect of steering deep brain stimulation. Brain Stimul. 2015; 8(4):730–41. [PubMed: 25753176]

Brittain JS, Brown P. Oscillations and the basal ganglia: motor control and beyond. Neuroimage. 2014; 85:637–47. [PubMed: 23711535]

Cagnan H, Pedrosa D, Little S, Pogosyan A, Cheeran B, Aziz T, et al. Stimulating at the right time: phase specific deep brain stimulation. Brain. 2017; 140:132–45. [PubMed: 28007997]

Chen CC, Pogosyan A, Zrinzo LU, Tisch S, Limousin P, Ashkan K, et al. Intra-operative recordings of local field potentials can help localize the subthalamic nucleus in Parkinson's disease surgery. Exp Neurol. 2006; 198(1):214–21. [PubMed: 16403500]

Cui Z, Pan L, Song H, Xu X, Xu B, Yu X, et al. Intraoperative MRI for optimizing electrode placement for deep brain stimulation of the subthalamic nucleus in Parkinson disease. J Neurosurg. 2016; 124(1):62–9. [PubMed: 26274983]

Doyle LMF, Kuhn AA, Hariz M, Kupsch A, Schneider GH, Brown P. Levodopa-induced modulation of subthalamic beta oscillations during self-paced movements in patients with Parkinson's disease. Eur J Neurosci. 2005; 21(5):1403–12. [PubMed: 15813950]

Eusebio A, Brown P. Oscillatory activity in the basal ganglia. Parkinsonism Relat Disord. 2007; 13(Suppl 3):S434–436. [PubMed: 18267278]

Eusebio A, Thevathasan W, Doyle Gaynor L, Pogosyan A, Bye E, Foltynie T, et al. Deep brain stimulation can suppress pathological synchronization in parkinsonian patients. J Neurol Neurosurg Psychiatr. 2011; 82:569–73.

Foffani G, Bianchi AM, Baselli G, Priori A. Movement-related frequency modulation of beta oscillatory activity in the human subthalamic nucleus. J Physiol. 2005; 568(2):699–711. [PubMed: 16123109]

Fogelson N, Pogosyan A, Kühn AA, Kupsch A, van Bruggen G, Speelman H, et al. Reciprocal interactions between oscillatory activities of different frequencies in the subthalamic region of patients with Parkinson's disease. Eur J Neurosci. 2005; 22:257–66. [PubMed: 16029215]

Fogelson N, Williams D, Tijssen M, van Bruggen G, Speelman H, Brown P. Different functional loops between cerebral cortex and the subthalmic area in Parkinson's disease. Cereb Cortex. 2006; 16(1):64–75. [PubMed: 15829734]

Hammond C, Bergman H, Brown P. Pathological synchronization in Parkinson's disease: networks, models and treatments. Trends Neurosci. 2007; 30(7):357–64. [PubMed: 17532060]

Hirschmann J, Özkurt TE, Butz M, Homburger M, Elben S, Hartmann CJ, et al. Distinct oscillatory STN-cortical loops revealed by simultaneous MEG and local field potential recordings in patients with Parkinson's disease. Neuroimage. 2011; 55(3):1159–68. [PubMed: 21122819]

Horn A, Kühn AA. Lead-DBS: a toolbox for deep brain stimulation electrode localizations and visualizations. Neuroimage. 2015; 107:127–35. [PubMed: 25498389]

Horn A, Neumann WJ, Degen K, Schneider GH, Kühn AA. Toward an electrophysiological "sweet spot" for deep brain stimulation in the subthalamic nucleus. Hum Brain Mapp. 2017; 38(7):3377–90.

Jakab A, Blanc R, Berenyi EL, Szekely G. Generation of individualized thalamus target maps by using statistical shape models and thalamocortical tractography. AJNR Am J Neuroradiol. 2012; 33:2110–6. [PubMed: 22700756]

Jenkinson N, Kühn AA, Brown P. Γ oscillations in the human basal ganglia. Exp Neurol. 2013; 245:72–6. [PubMed: 22841500]

Joundi RA, Brittain JS, Green AL, Aziz TZ, Brown P, Jenkinson Ned. Oscillatory activity in the subthalamic nucleus during arm reaching in Parkinson's disease. Exp Neurol. 2012; 236(2):319–26. [PubMed: 22634757]

Klostermann F, Nikulin VV, Kühn AA, Marzinzik F, Wahl M, Pogosyan A, et al. Task-related differential dynamics of EEG alpha- and beta-band synchronization in cortico-basal motor structures. Europ J Neurosci. 2007; 25(5):1604–15.

Kolb R, Abosch A, Felsen G, Thompson JA. Use of intraoperative local field potential spectral analysis to differentiate basal ganglia structures in Parkinson's disease patients. Physiol Rep. 2017; 5(12): 1–14.

Kühn AA, Williams D, Kupsch A, Limousin P, Hariz M, Schneider GH, et al. Event-related beta desynchronization in human subthalamic nucleus correlates with motor performance. Brain. 2004; 127(4):735–46. [PubMed: 14960502]

Kühn AA, Kempf F, Brucke C, Gaynor Doyle L, Martinez-Torres I, Pogosyan A, et al. High-frequency stimulation of the subthalamic nucleus suppresses oscillatory beta activity in patients with Parkinson's disease in parallel with improvement in motor performance. J Neurosci. 2008; 28:6165–73. [PubMed: 18550758]

Kühn AA, Tsui A, Aziz T, Ray N, Bruecke C, Kupsch A, et al. Pathological synchronisation in the subthalamic nucleus of patients with Parkinson's disease relates to both bradykinesia and rigidity. Exp Neurol. 2009; 215(2):380–7. [PubMed: 19070616]

Kullback S, Leibler RA. On information and sufficiency. Ann Math Stat. 1951; 22:79–86.

Lalo E, Gilbertson T, Doyle L, Di Lazzaro V, Cioni B, Brown P. Phasic increases in cortical beta activity are associated with alterations in sensory processing in the human. Exp Brain Res. 2007; 177(1):137–45. [PubMed: 16972074]

Levy R, Ashby P, Hutchison WD, Lang AE, Lozano AM, Dostrovsky JO. Dependence of subthalamic nucleus oscillations on movement and dopamine in Parkinson's disease. Brain. 2002; 125:1196–209. [PubMed: 12023310]

Little SJ, Pogosyan A, Neal S, Zavala B, Zrinzo L, Hariz M, et al. Adaptive deep brain stimulation in advanced Parkinson's disease. Ann Neurol. 2013; 74:449–57. [PubMed: 23852650]

Litvak V, Jha A, Eusebio A, Oostenveld R, Foltynie T, Limousin P, et al. Resting oscillatory cortico-subthalamic connectivity in patients with Parkinson's disease. Brain. 2011; 134:359–74. [PubMed: 21147836]

Logothetis NK. The underpinnings of the BOLD functional magnetic resonance imaging signal. J Neurosci. 2003; 23:3963–71. [PubMed: 12764080]

Lourens MAJ, Meijer HE, Contarino MF, van den Munckhof P, Schuurman PR, van Gils SA, et al. Functional neuronal activity and connectivity within the subthalamic nucleus in Parkinson's disease. Clin Neurophysiol. 2013; 124:967–81. [PubMed: 23182834]

Marmor O, Valsky D, Joshua M, Bick AS, Arkadir D, Tamir I, et al. Local vs. volume conductance activity of field potentials in the human subthalamic nucleus. J Neurophysiol. 2017; 117(6):2140–51. [PubMed: 28202569]

Mestre TA, Lang AE, Okun MS. Factors influencing the outcome of deep brain stimulation: placebo, nocebo, lessebo, and lesion effects. Mov Disord. 2016; 31:290–8. [PubMed: 26952118]

Michmizos KP, Frangou P, Stathis P, Sakas D, Nikit KS. Beta-band frequency peaks inside the subthalamic nucleus as a biomarker for motor improvement after deep brain stimulation in Parkinson's disease. IEEE J Biomed Health Inform. 2015; 19(1):174–80. [PubMed: 25095273]

Miyagi Y, Okamoto T, Morioka T, Tobimatsu S, Nakanishi Y, Aihara K, et al. Spectral analysis of field potential recordings by deep brain stimulation electrode for localization of subthalamic nucleus in

patients with Parkinson's disease. Stereotact Funct Neurosurg. 2009; 87(4):211–8. [PubMed: 19571612]

Morel, A. Stereotactic atlas of the human thalamus and basal ganglia. Boca Raton: CRC Press; 2013.

Pollo C, Kaelin-Lang A, Oertel MF, Stieglitz L, Taub E, Fuhr P, et al. Directional deep brain stimulation: an intraoperative double-blind pilot study. Brain. 2014; 137:2015–26. [PubMed: 24844728]

Ray NJ, Jenkinson N, Wang S, Holland P, Brittain JS, Joint C, et al. Local field potential beta activity in the subthalamic nucleus of patients with Parkinson's disease is associated with improvements in bradykinesia after dopamine and deep brain stimulation. Exp Neurol. 2008; 213(1):108–13. [PubMed: 18619592]

Reck C, Florin E, Wojtecki L, Groiss S, Voges J, Sturm V, et al. Differential distribution of coherence between beta-band subthalamic oscillations and forearm muscles in Parkinson's disease during isometric contraction. Clin Neurophysiol. 2009; 120(8):1601–9. [PubMed: 19564131]

Rodriguez-Oroz MC, Lopez-Azcarate J, Garcia-Garcia D, Alegre M, Toledo J, Valencia M, et al. Involvement of the subthalamic nucleus in impulse control disorders associated with Parkinson's disease. Brain. 2011; 134:36–49. [PubMed: 21059746]

Sburlea, AI., Montesano, L., Minguez, J. Intersession adaptation of the EEG-based detector of self-paced walking intention in stroke patients. Conf Proc IEEE Eng Med Biol Soc; 2015. p. 498-501.

Shimamoto SA, Ryapolova-Webb ES, Ostrem JL, Galifianakis NB, Miller KJ, Starr PA. Subthalamic nucleus neurons are synchronized to primary motor cortex local field potentials in Parkinson's disease. J Neurosci. 2013; 33:7220–33. [PubMed: 23616531]

Steiner LA, Neumann WJ, Staub-Bartelt F, Herz DM, Tan H, Pogosyan A, et al. Subthalamic beta dynamics mirror Parkinsonian bradykinesia months after neurostimulator implantation. Mov Disord. 2017; 32:1183–90. [PubMed: 28639263]

Swann NC, de Hemptinne C, Miocinovic S, Qasim S, Wang SS, Ziman N, et al. Gamma oscillations in the hyperkinetic state detected with chronic human brain recordings in Parkinson's disease. J Neurosci. 2016; 36(24):6445–58. [PubMed: 27307233]

Tan H, Pogosyan A, Ashkan K, Cheeran B, FitzGerald JJ, Green AL, et al. Frequency specific activity in subthalamic nucleus correlates with hand bradykinesia in Parkinson's disease. Exp Neurol. 2013; 240:122–9. [PubMed: 23178580]

Timmermann L, Jain R, Chen L, Marrouf M, Barbe MT, Allert N, et al. Multiple-source current steering in subthalamic nucleus deep brain stimulation for Parkinson's disease (the VANTAGE study): A non-randomised, prospective, multicentre, open-label study. Lancet Neurol. 2015; 14:693–701. [PubMed: 26027940]

Tinkhauser G, Pogosyan A, Debove I, Nowacki A, Shah SA, Seidel K, et al. Directional local field potentials: a tool to optimize deep brain stimulation. Mov Disord. 2017; doi: 10.1002/mds.27215

Verhagen R, Zwartjes DGM, Heida T, Wiegers EC, Contarino MF, de Bie RMA, et al. Advanced target identification in STN-DBS with beta power of combined local field potentials and spiking activity. J Neurosci Methods. 2015; 253:116–25. [PubMed: 26079495]

Welch PD. The use of Fast Fourier Transform for the estimation of power spectra: a method based on time averaging over short, modified periodograms. IEEE Trans Audio Electroacoustics. 1967; 15:70–3.

Weinberger M, Hutchison WD, Lozano AM, Hodaie M, Dostrovsky JO. Increased gamma oscillatory activity in the subthalamic nucleus during tremor in Parkinson's disease patients. J Neurophysiol. 2009; 101:789–802. [PubMed: 19004998]

Yoshida F, Martinez-Torres I, Pogosyan A, Holl E, Petersen E, Chen CC, et al. Value of subthalamic nucleus local field potentials recordings in predicting stimulation parameters for deep brain stimulation in Parkinson's disease. J Neurol Neurosurg Psychiatry. 2010; 81(8):885–9. [PubMed: 20466699]

Europe PMC Funders Author Manuscripts

Highlights

- The 3-D visualized subthalamic area and the local field potential (LFP) oscillations were estimated intraoperatively.
- The resting and movement modulated oscillations had focal maxima in frequency bands.
- Movement related modulations showed differences in the scale and timing across frequency bands.

Europe PMC Funders Author Manuscripts

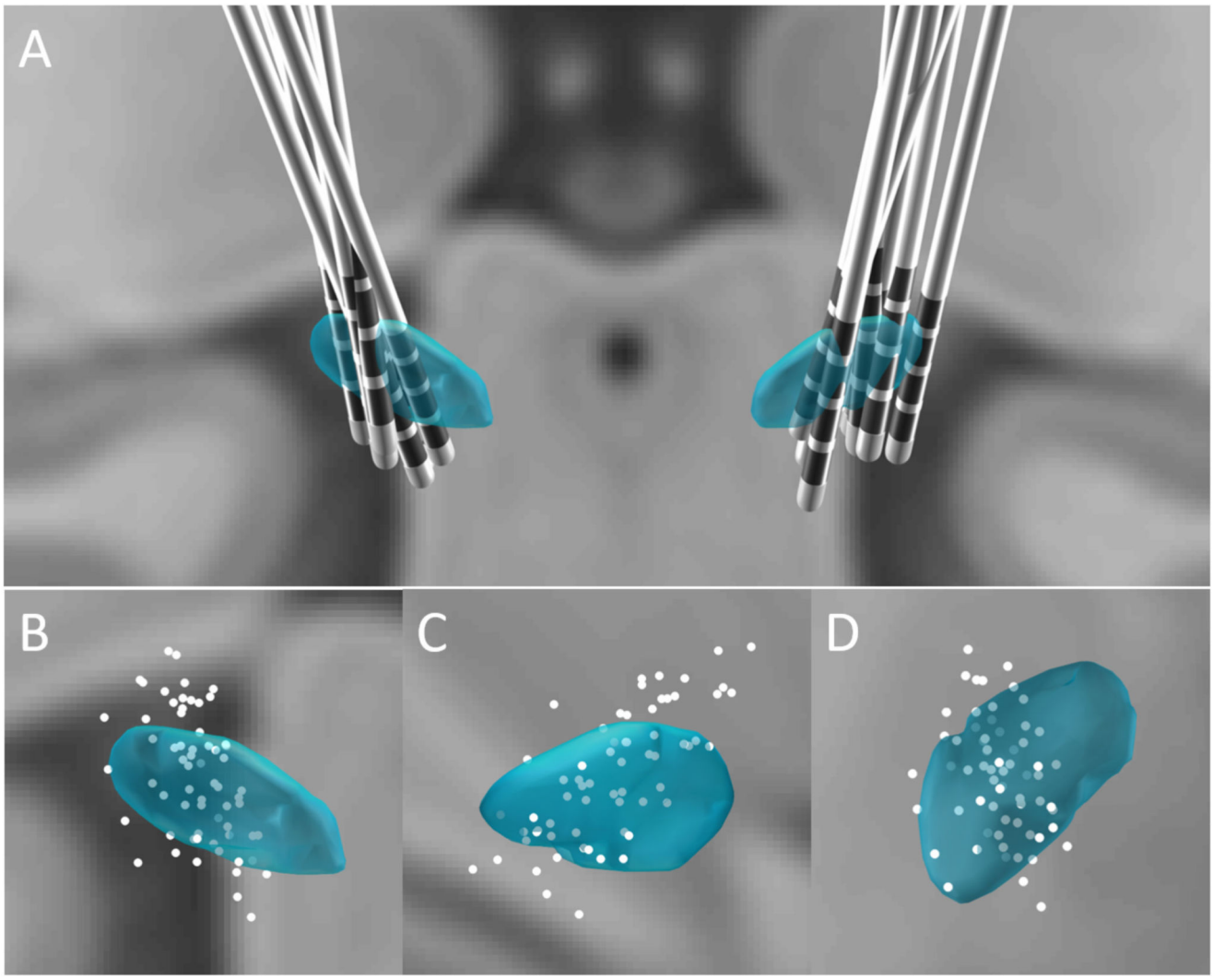

Fig. 1.

Group distribution of DBS electrodes (A) of all 16 sides in the 8 subjects and the coordinates of all individual contacts in coronal view (B), sagittal view (C) and transverse view (D). STN is represented in blue and contacts are represented as white dots.

Europe PMC Funders Author Manuscripts

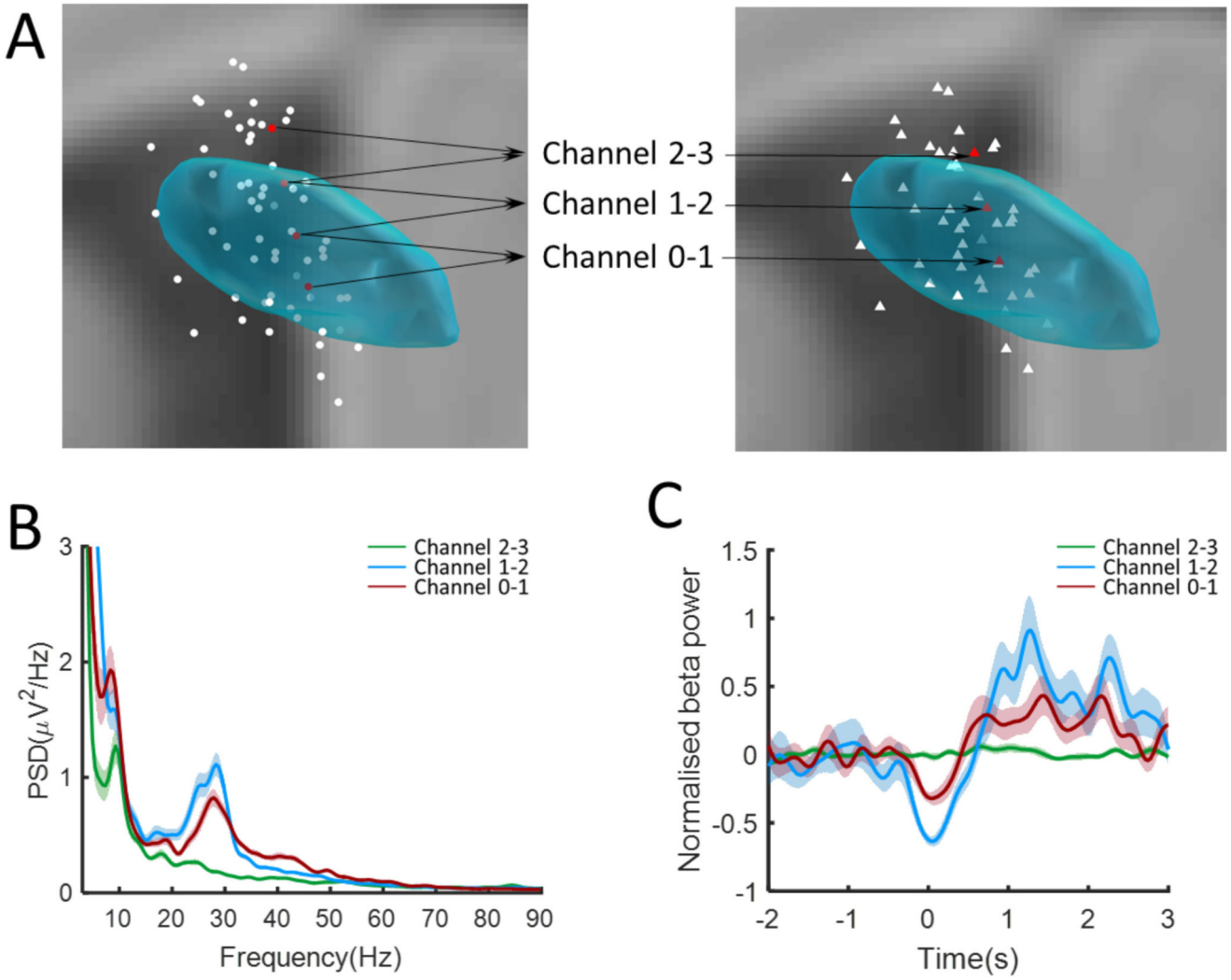

Fig. 2.

Example to show the distribution of resting and movement modulated oscillations. (A) Coordinates of the three bipolar LFPs channels (right) recorded from four contacts (left) of left STN in case 4. Coordinates of the bipolar channels are taken as the middle points between the corresponding contact pairs (B) Spectral power of resting oscillations over 3–90 Hz. That in the beta frequency (13–32 Hz) in channel 2–3 (green line and shadow) located dorsally outside STN is lower than that in channels 1–2 and 0–1 located inside of STN. (C) Movement modulated beta (13–32 Hz) oscillations in a −2 to 3 s window re-aligned to the time of response. The movement modulation in the beta band in the dorsal channel outside of STN is weaker than that inside of STN.

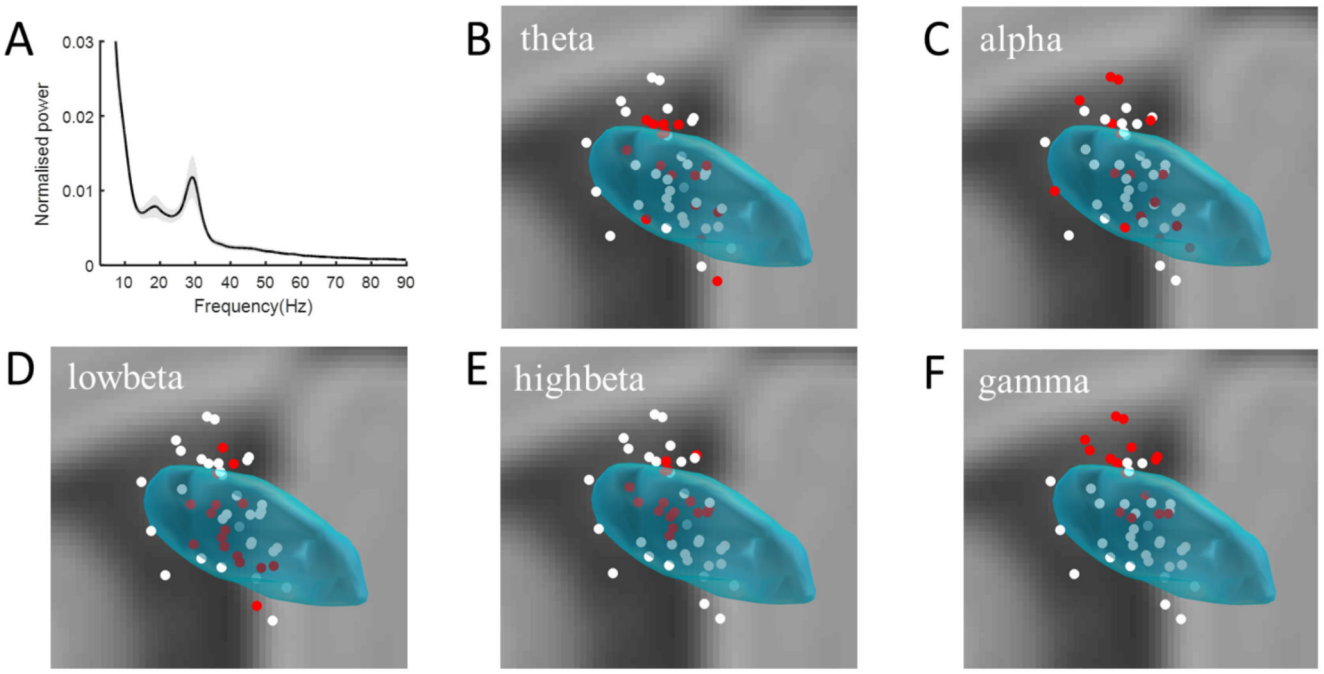

Fig. 3.

Group power spectral density over 3–90 Hz averaged across all recording channels (A). Shading represents ± Standard Deviation (SD) of all z-score normalised power data. Distributions of normalised resting power in the theta (4–8 Hz, B), alpha (8–12 Hz, C), low beta (13–20 Hz, D), high beta (21–32 Hz, E) and high gamma (60–90 Hz, F) bands in coronal view. The white dots in panels B-F represent the location of all bipolar contact-pairs (as defined in Fig. 3A). The red dots represent the sixteen contact-pairs which had the highest normalised spectral power in each frequency band across the group.

Europe PMC Funders Author Manuscripts

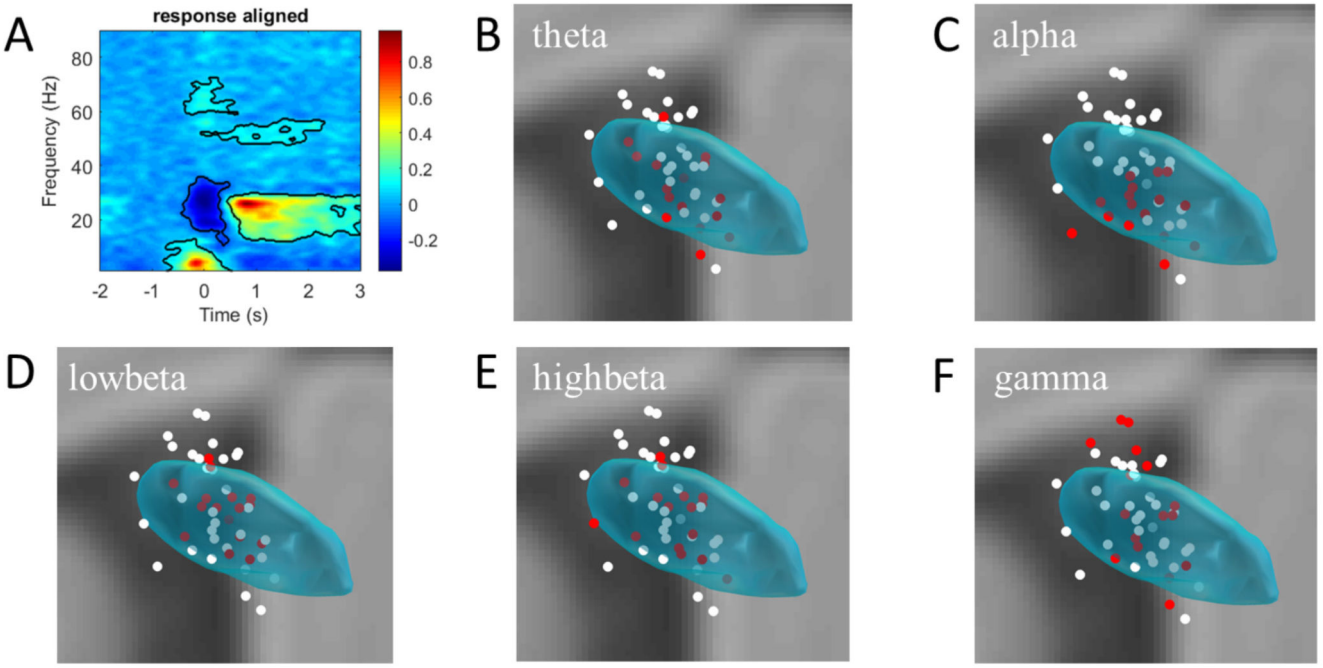

Fig. 4.

Normalised and group averaged time-frequency (3–90 Hz) spectrogram in a −2 to 3 s window re-aligned to the onset of movement (A). The cluster surrounded regions denote that the movement modulated power increased and decreased with statistical significance. Distributions of the significantly modulated power in the theta (4–8 Hz, B), alpha (8–12 Hz, C), low beta (16–20 Hz, D), high beta (21–36 Hz, E) and gamma (59–73 Hz, F) bands are illustrated in coronal views. Filled dots in panels B-F represent the location of all contact-pairs (taken as the middle point of each pair). The red dots represent the coordinates of the 16 contact-pairs which had the greatest modulation of power in each frequency band across the group.

Europe PMC Funders Author Manuscripts

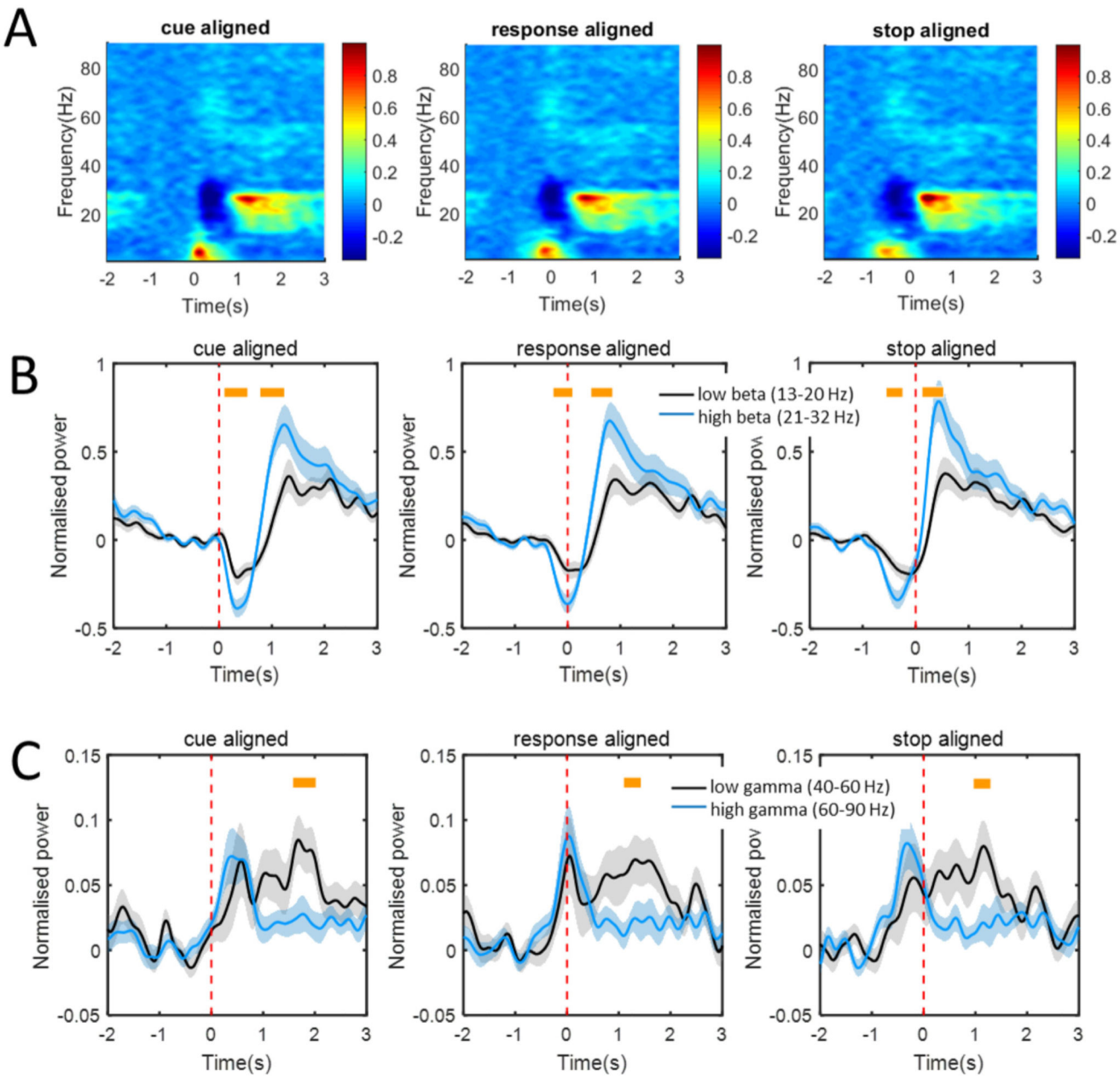

Fig. 5.

Normalised movement modulated power changes of oscillations. (A) Normalised time-frequency spectra of the movement modulated oscillations over 3–90 Hz in a −2 to 3 s window aligned to the time (0 s) of cue, response onset and end of the movement. Power increases were found over alpha and gamma bands and power decreases were found over low beta and high beta bands at the time of movement response. Also, a post-movement power increase was found in the low and high beta bands, and in the low gamma frequency band. (B) Normalised power changes over low beta (black lines and shadows) and high beta (blue lines and shadows) bands aligned to the time of cue, response onset and end of movement. (C) Normalised power changes over low gamma (black lines and shadows) and

high gamma (blue lines and shadows) bands aligned to the time of cue, response onset and end of movement. Significant differences in amplitudes of movement modulations are marked by yellow bars ($p < 0.01$, paired t-test). Shading represents ± standard error of the mean power change.

Europe PMC Funders Author Manuscripts

Europe PMC Funders Author Manuscripts

Table 1

Clinical summary.

Case	Age/sex	Dominant symptoms	Duration of disease (years)	UPDRS part-III (pre-operative off medication)
1	50/M	Right side rigidity and tremor; left side rigidity	4	38
2	55/M	Left side rigidity and tremor	10	52
3	49/M	Tremor, rigidity and bradykinesia	2	53
4	65/F	Rigidity, mobility and gait impairment	7	54
5	52/M	Rigidity and bradykinesia	5	40
6	45/F	Bradykinesia and gait impairment	N/A	41
7	64/M	Tremor	N/A	N/A
8	57/M	Rigidity, tremor and dyskinesia	4	57

UPDRS = Unified Parkinson's disease rating scale. Part – III: Motor Exam.

Europe PMC Funders Author Manuscripts

Table 2

Variance tests of the Euclidean distances of power distributions at rest and during movement.

	Resting F(1127, 119)	Resting *P*-value	Euclidean distance (Mean ± SD) (mm)	Resting sides/ subjects	Movement F(1127, 119)	Movement *P*-value	Euclidean distance (Mean ± SD) (mm)	Movement side/subjects
Theta	0.8904	0.3674	3.9 ± 2.0	13/8	1.2132	0.1790	3.8 ± 1.7	13/8
Alpha	0.7115	**0.0081**	4.8 ± 2.2	13/8	1.5342	**0.0034**	3.4 ± 1.5	14/8
Low beta	1.6513	**6.6861e−04**	3.3 ± 1.4	12/8	1.8554	**3.5150e−05**	3.3 ± 1.5	15/8
High beta	4.3026	**1.0164e−18**	2.4 ± 0.9	12/8	1.5653	**0.0022**	3.5 ± 1.5	12/7
gamma	1.9663	**6.9584e−06**	3.2 ± 1.3	14/8	0.7378	**0.0183**	4.3 ± 2.2	15/8

Data are from the 16 contact-pairs with the highest relative power in each band from across the group. The total number of sides and patients from which these are drawn are also given. Theta, alpha, low beta, high beta and gamma were taken as 4–8 Hz, 8–12 Hz, 13–20 Hz, 21–32 Hz, and 60–90 Hz during rest and 4–8 Hz, 8–12 Hz, 16–20 Hz, 21–36 Hz and 59–73 Hz during movement, respectively. *P*-values in bold are significant following correction for multiple comparisons using the false discovery rate, and, when interpreted in terms of the difference in the subgroup mean Euclidean distance relative to that of the whole group (4.0 ± 1.9 mm), determine whether subgroups were more, or less, distributed in space than the master group of all 48 contacts.